From Zero- to One-Dimensional, Opportunities and Caveats of Hybrid Iodobismuthates for Optoelectronic Applications

Alla Skorokhod,[1] Nicolas Mercier,[1,*] Magali Allain,[1] Matthieu Manceau,[2] Claudine Katan,[3] and Mikaël Kepenekian[3,‡]

[1]*MOLTECH-Anjou, UMR-CNRS 6200, Université d'Angers, 49045 Angers, France*
[2]*Department of Solar Technologies, INES, CEA, LITEN, Université Grenoble Alpes, F-73375 Le Bourget du Lac, France*
[3]*Univ Rennes, ENSCR, INSA Rennes, CNRS, ISCR – UMR 6226, F-35000 Rennes, France*

Emails: nicolas.mercier@univ-angers.fr; mikael.kepenekian@univ-rennes1.fr

Supporting Information

Table of contents

Synthesis of 1,1'-diamino-4,4'-bipyridinium iodide

The synthesis of 4-carboxy-1-methylpyridinium iodide was made according to the literature.[1] 4,4'-bipyridine (3.9 g, 0.025 mol) was dissolved in 15 ml of water, stirring at 70°C. A solution of Hydroxylamine-O-sulfonic acid (5.67 g; 0.05 mol in 10 ml H_2O), previously neutralized at -5 °C with KOH water solution (10 ml, 5M), was added dropwise. The reaction mixture was cooled to room temperature. Then a concentrated K_2CO_3 solution (3.45 mg; 5 ml H_2O) was added. The potassium sulfate was precipitated by addition 150 ml of methanol and filtered off. After, a concentrated aqueous solution of HI (57%) was gradually added to the yellow filtrate, till the pH was reduced to 5. The resulting golden-yellow precipitate of 1,1'-diamino-4,4'-bipyridinium iodide was filtered off and washed with acetone. The yield is 88.5%. ^{1}H NMR (300 MHz, DMSO) δ 8.93(d, *J*=7.2 Hz, 1H), 8.49, (d, *J*=7.2Hz, 1H).

[1] Szafran, M.; Koput, J.; Dega-Szafran, Z.; Katrusiak, A. *J. Mol. Struc.* **2006,** *797*, 66-81.

Table S1. Crystallographic data and structure refinement parameters for $(AmV)_3(BiI_6)_2$.

Empirical formula	C15 H18 Bi I6 N6
Formula weight	1252.73
Temperature	293(2) K
Wavelength	1.54184 Å
Crystal system, space group	Triclinic, P -1
Unit cell dimensions	a = 8.4259(4) Å alpha = 89.524(4) deg. b = 12.6618(7) Å beta = 85.807(4) deg. c = 12.7182(6) Å gamma = 81.320(4) deg.
Volume	1337.73(12) $Å^3$
Z, Calculated density	2, 3.110 Mg/m^3
Absorption coefficient	67.412 mm^{-1}
F(000)	1102
Crystal size	0.030 x 0.032 x 0.067 mm
Theta range for data collection	3.484 to 73.010 deg.
Limiting indices	-8<=h<=10, -15<=k<=15, -15<=l<=15
Reflections collected / unique	7863 / 5031 [$R_{(int)}$ = 0.0348]
Completeness to theta = 70.000	96.8 %
Refinement method	Full-matrix least-squares on F^2
Data / restraints / parameters	5031 / 6 / 256
Goodness-of-fit on F^2	1.086
Final R indices [I>2sigma(I)]	R_1 = 0.0437, wR2 = 0.1171
R indices (all data)	R_1 = 0.0495, wR2 = 0.1330
Extinction coefficient	n/a
Largest diff. peak and hole	1.653 and -3.268 e.A^-3

Table S2. Crystallographic data and structure refinement parameters for $(AmV)_2(Bi_4I_{16})$.

Empirical formula	C10 H12 Bi2 I8 N4
Formula weight	1621.40
Temperature	298(4) K
Wavelength	1.54184 Å
Crystal system, space group	Triclinic, P -1
Unit cell dimensions	a = 10.3705(7) Å alpha = 69.660(7) deg. b = 11.6684(9) Å beta = 67.575(7) deg. c = 13.2140(10) Å gamma = 85.168(6) deg.
Volume	1383.8(2) $Å^3$
Z, Calculated density	2, 3.891 Mg/m^3
Absorption coefficient	94.786 mm^{-1}
F(000)	1380
Crystal size	0.094 x 0.176 x 0.398 mm
Theta range for data collection	3.852 to 72.615 deg.
Limiting indices	-12<=h<=10, -14<=k<=12, -16<=l<=9
Reflections collected / unique	9191 / 5305 [$R_{(int)}$ = 0.0448]
Completeness to theta = 70.000	98.6 %
Refinement method	Full-matrix least-squares on F^2
Data / restraints / parameters	5305 / 0 / 217
Goodness-of-fit on F^2	1.050
Final R indices [I>2sigma(I)]	R_1 = 0.0478, wR2 = 0.1258
R indices (all data)	R_1 = 0.0532, wR2 = 0.1373
Extinction coefficient	n/a
Largest diff. peak and hole	3.350 and -2.521 e.A^-3

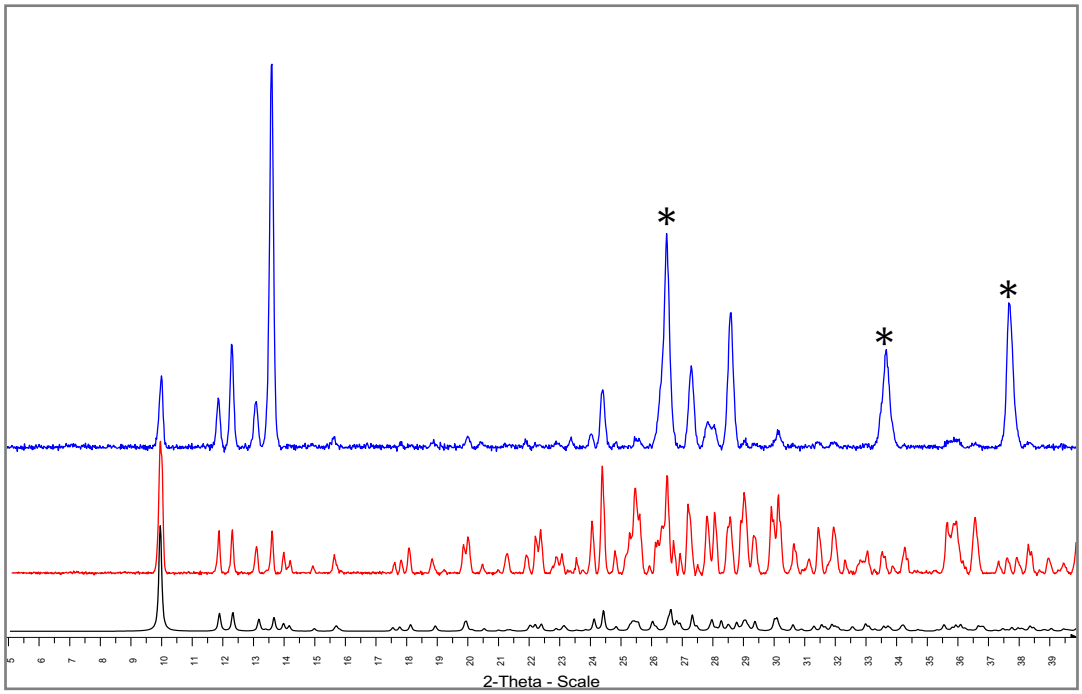

Figure S1. PXRD Patterns of $(AmV)_3(BiI_6)_2$: simulated (black line); experimental diffractogram of powder (red line); experimental diffractogram of thin film (blue line) deposed on a layer of FTO (*).

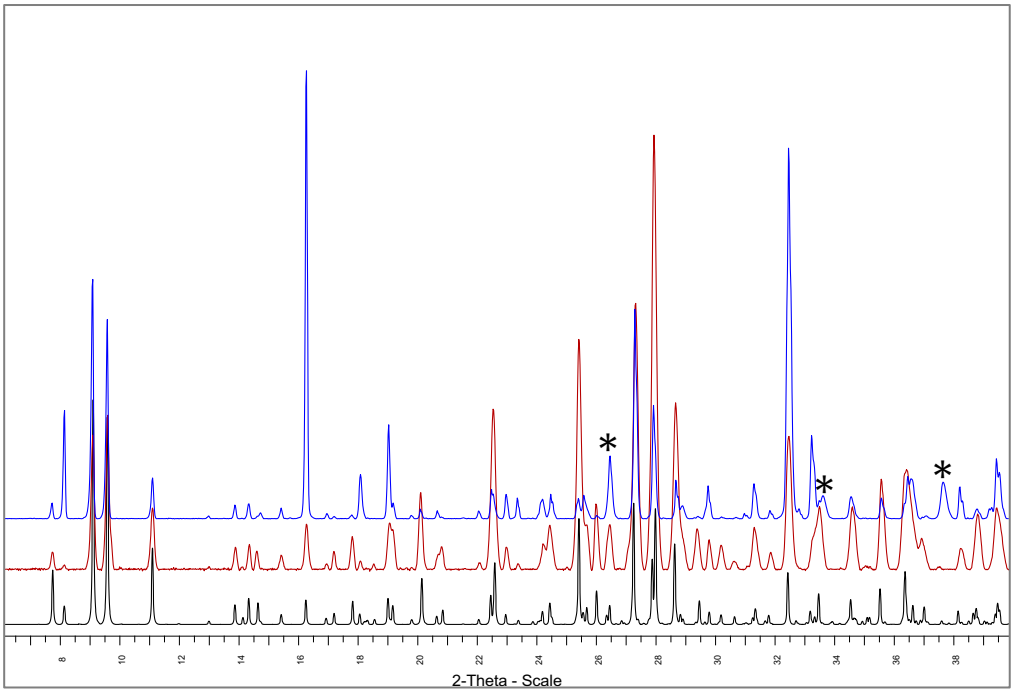

Figure S2. PXRD Patterns of $(AmV)_2(Bi_4I_{16})$: simulated (black line); experimental diffractogram of powder (red line); experimental diffractogram of thin film (blue line) deposed on a layer of FTO (*).

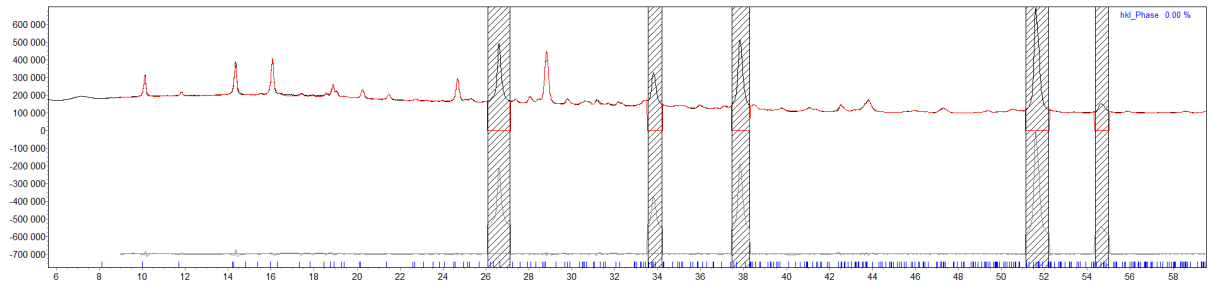

Figure S3. (AmV)BiI_5: PXRD pattern (black line); Profile fitting* (red line) and difference (gray line). Gray boxes correspond to FTO lines.

***Result of profile fitting refinements**

R-Values

Rexp : 0.24 Rwp : 1.45 Rp : 1.08 GOF : 6.10

Rexp`: 1.75 Rwp`: 10.67 Rp` : 12.38 DW : 0.25

Background

Chebychev polynomial, Coefficient 0 137358 ; 1 -56718.74 ; 2 5807.854

3 10401.17 ; 4 -9248.687 ; 5 920.5282 ; 6 -4408.853 ; 7 -1083.094

Instrument

Primary radius (mm)	217.5
Secondary radius (mm)	217.5

Corrections

Zero Error	0.1

Miscellaneous

Start X	9	
Finish X	60	
Excluded Regions (FTO lines)		
Start/Finish	26.1	27.12
Start/Finish	33.55	34.2
Start/Finish	37.45	38.27
Start/Finish	51.15	52.21
Start/Finish	54.36	55

Pawley method

R-Bragg	38.796
Spacegroup	P21
Cell Volume (Å^3)	1046.7
Lattice parameters *	
a (Å)	6.367
b (Å)	15.106
c (Å)	11.128
beta (°)	102.071

Crystallite Size

Cry Size Lorentzian (nm)	85.1

* The unit cell parameters, obtained from a single-crystal study of a very thin crystal (200 K), are: a= 6.385(4) Å; b = 15.166(7) Å; c = 11.052(4) Å; beta = 102.57(5)°; V= 1044.6(9) $Å^3$.

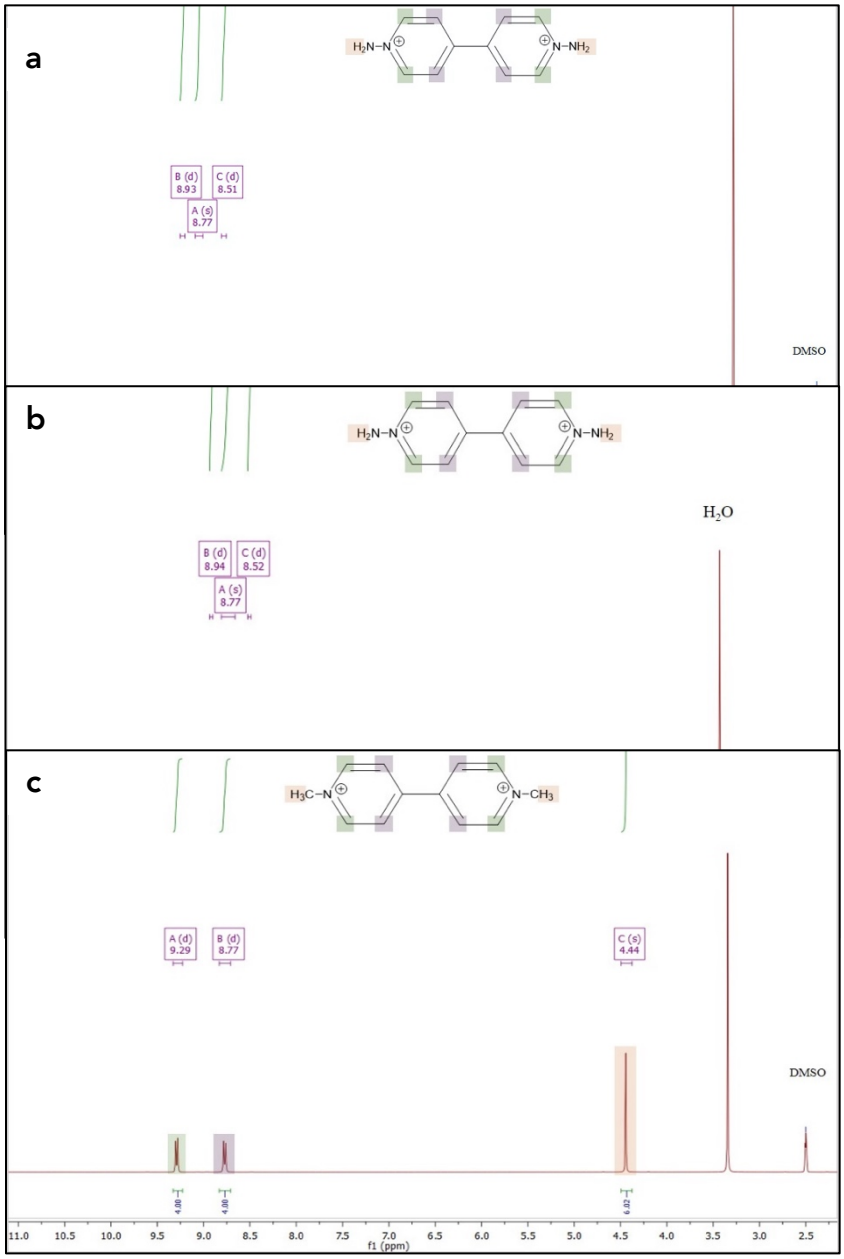

Figure S4. ^{1}H NMR (300 MHz, DMSO) of (AmV)BiI_5 (a): δ 8.93 (d, *J* = 7.2 Hz, 4H), 8.77 (s, 4H), 8.51 (d, *J* = 7.2 Hz, 4H); (AmV)I_2 (b): δ 8.94 (d, *J* = 7.2 Hz, 4H), 8.77 (s, 4H), 8.52 (d, *J* = 7.2 Hz, 4H); and (MV)I_2 (c, MV= methylviologen): δ 9.29 (d, *J* = 6.8 Hz, 4H), 8.77 (d, *J* = 6.9 Hz, 4H), 4.44 (s, 6H).

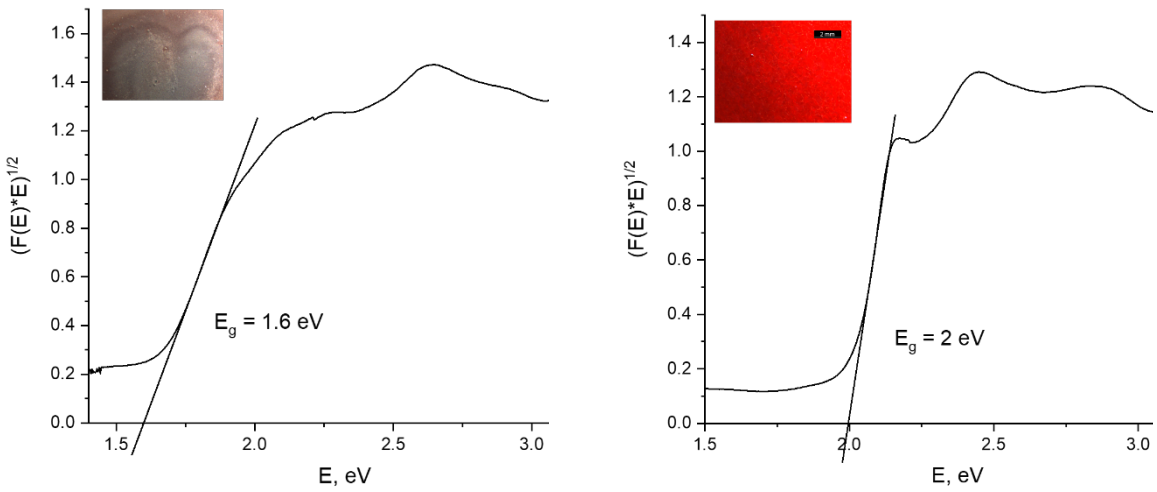

Figure S5. Tauc plot for compounds/thin films **1** (left) and **2** (right) (indirect band gap).

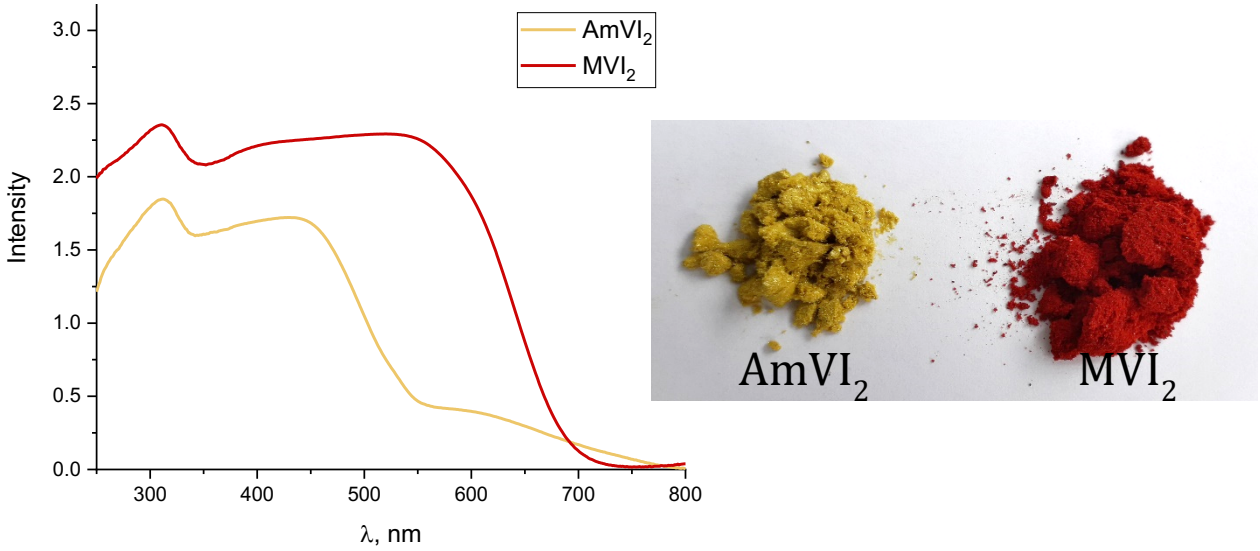

Figure S6. Absorbance spectra (left) and photo of crystallized powders of $AmVI_2$ nd MVI_2 (MV= methylviologen)).

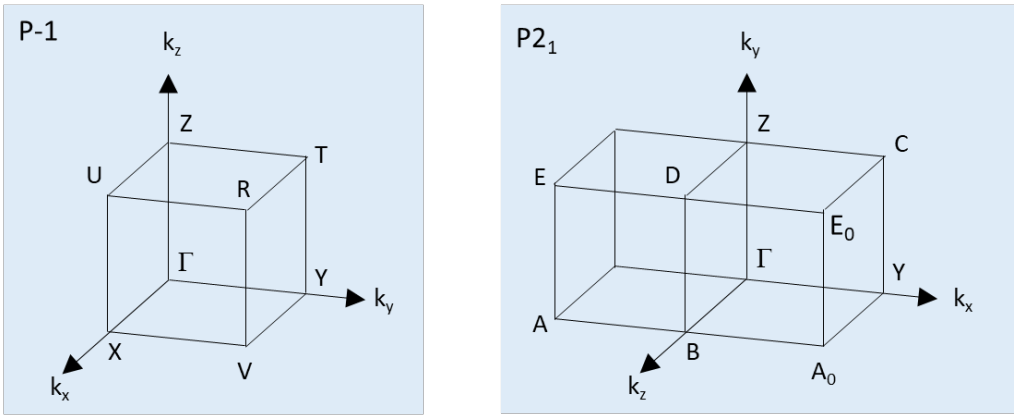

Figure S7. Brillouin zones for P-1 and $P2_1$ crystal groups used for $(AmV)_3(BiI_6)_2$ (**1**) and $(AmV)_2(Bi_4I_{16})$ (**2**), and $(Amv)BiI_5$ (**3**), respectively.

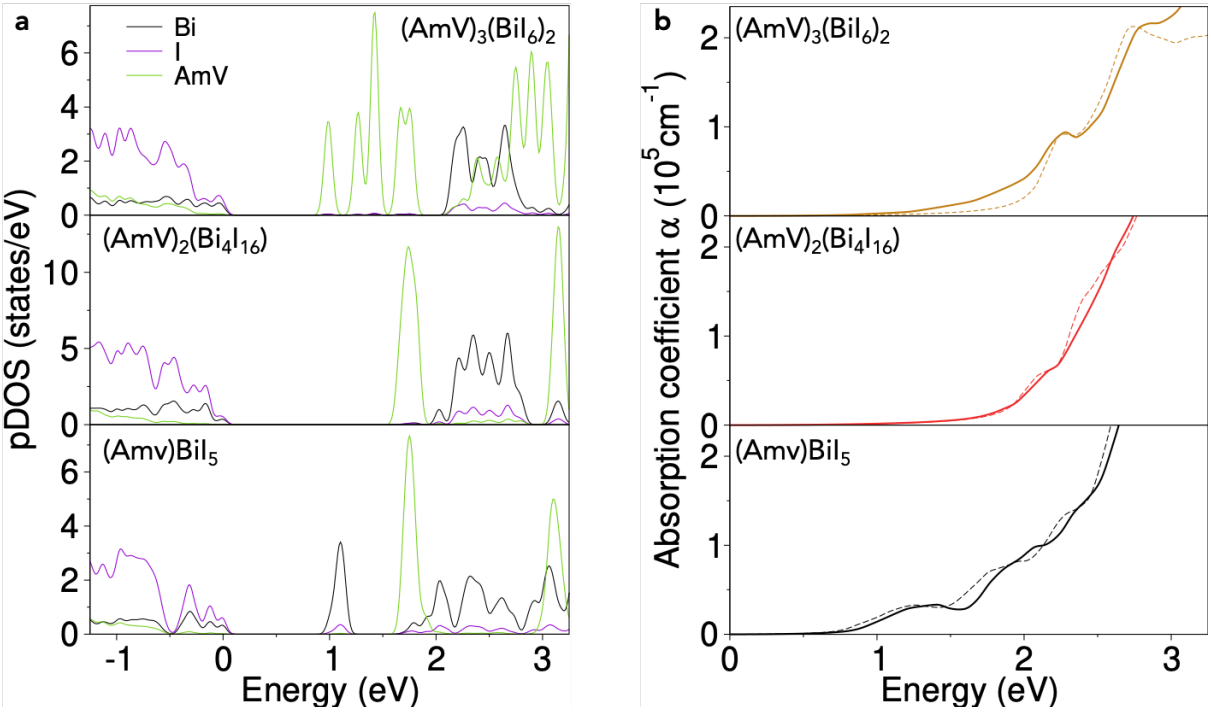

Figure S8. (a) Project density of states (pDOS) computed at the HSE06 level for (top) $(AmV)_3(BiI_6)_2$ (**1**), (middle) $(AmV)_2(Bi_4I_{16})$ (**2**), and (bottom) $(Amv)BiI_5$ (**3**). The origin of the energy scale is taken at the top of the valence band. (b) Corresponding computed absorption coefficient ⍰⍰

Table S3. Summary of computational results (GGA and HSE06) for $(AmV)_3(BiI_6)_2$ (**1**) and $(AmV)_2(Bi_4I_{16})$ (**2**), $(Amv)BiI_5$ (**3**) and the cis-connected system $(DMES)BiI_5$.

	$(AmV)_3(BiI_6)_2$	$(AmV)_2Bi_4I_{16}$	$(AmV)BiI_5$		$(DMES)BiI_5$
Band gap (full system)	Direct @ V	Indirect Z→X	Direct @ Y		
Band gap (inorganic lattice)	Indirect V→U	Direct @ Z	Direct @ Y		Direct @ R
GGA E_G (eV)	0.12	0.71	0.50		
GGA Inorganic lattice E_G (eV)	1.30	1.26	0.50		0.74
HSE06 E_G (eV)	0.96	1.65	1.00		
HSE06 Inorganic lattice E_G (eV)	2.15	2.02	1.00		
			$m_\perp$	$m_\parallel$	$m_\parallel$
GGA hole (m_0)	–0.280	–0.400	–0.150	–2.800	–0.270
GGA electron (m_0)	0.240	0.310	0.340	0.060	0.200

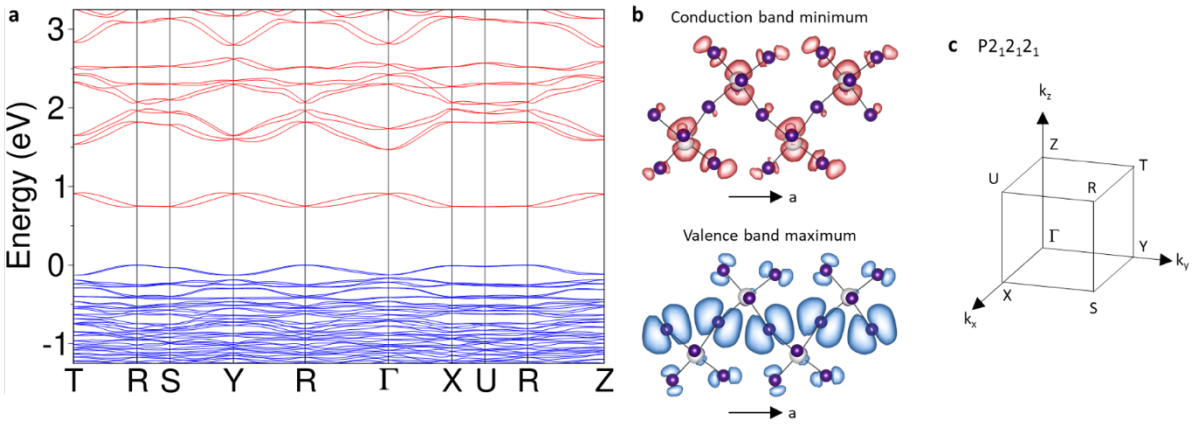

Figure S9. Electronic structure of *zigzag cis-BiI_5* networks. (a) Band structure of $(DMES)BiI_5$ computed using the revPBE functional and a background charge to mimic the effect of organic cations. The origin of the energy scale is taken at the top of the valence band. (b) Wavefunction modulus taken at the valence band maximum (blue, bottom) and conduction band minimum (top, red). (c) Brillouin zone of the $P2_12_12_1$ group. Because of the zigzag *cis-connected* configuration of the BiI_5 chain, a coupling is observed between central iodides leading to a ten times smaller hole effective mass in the direction of the wire than with the *trans-connected* configuration. By contrast, at the conduction band minimum, the coupling is lesser in the *cis* than in the *trans-BiI_5 network* and the electron effective mass increases by a factor 3.

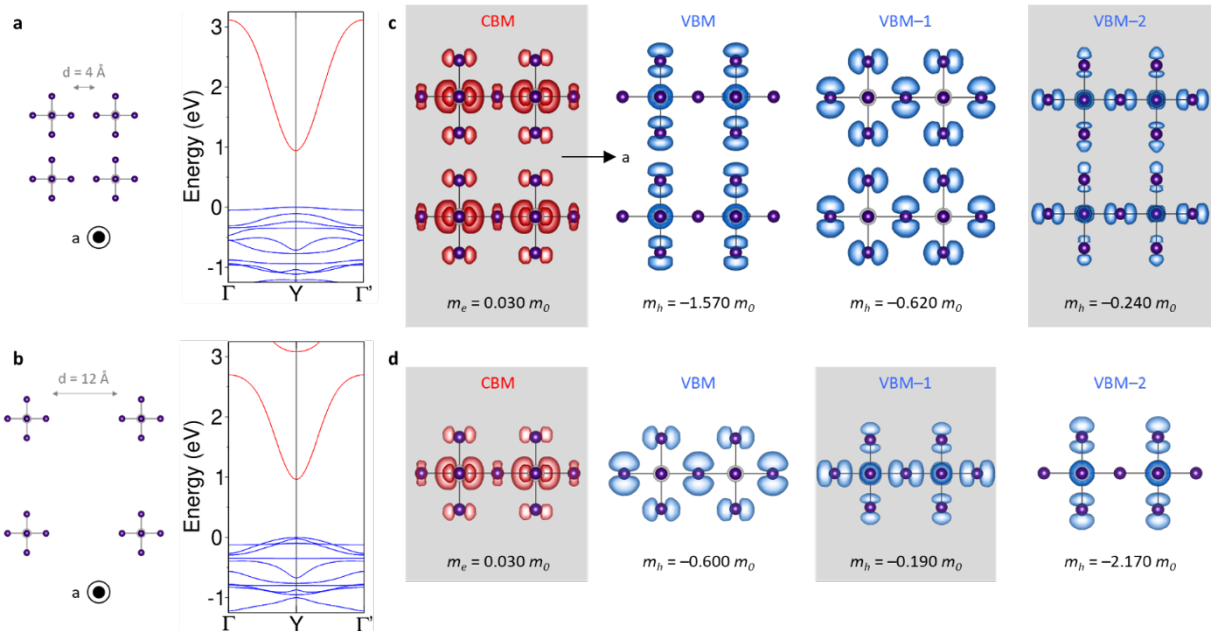

Figure S10. Electronic properties of trans-connected BiI_5 model structures. (a) Band structure of the model BiI_5-chains with short 4 Å inter-chain distance computed using the revPBE functional and a background charge to mimic the effect of organic cations. The origin of the energy scale is taken at the top of the valence band. (b) Same with the model BiI_5-chains with increased (12 Å) inter-chain distance. (c) Wavefunctions modulus taken at the conduction band maximum (red), valence band maximum (blue) and next lower lying valence bands (blue) computed for the 4 Å model. The corresponding electron and hole effective masses are given below. (d) Same for the 12 Å model. Considering the large distance between chains, only a single chain is depicted. The gray areas mark states with low effective masses. In both configurations, CBMs consist in overlapping Bi($6p_x$) orbitals leading to highly dispersive bands and small electron effective masses. In the short inter-chain distance model, the VBM consists in inter-chain couplings between dangling iodides. As a consequence, there is no contribution in the chain direction and, thus, a large hole effective mass along the chain. In the long-distance model, this valence state is lowered in energy and the VBM is formed by intra-chain electronic couplings. However, the coupling between I($5p_x$) and Bi($6s$) orbitals that leads to strong band dispersion and lower hole effective mass is not the top valence band. Thus, the hole transporting properties of the isolated *trans*-connected BiI_5 chains remain limited.

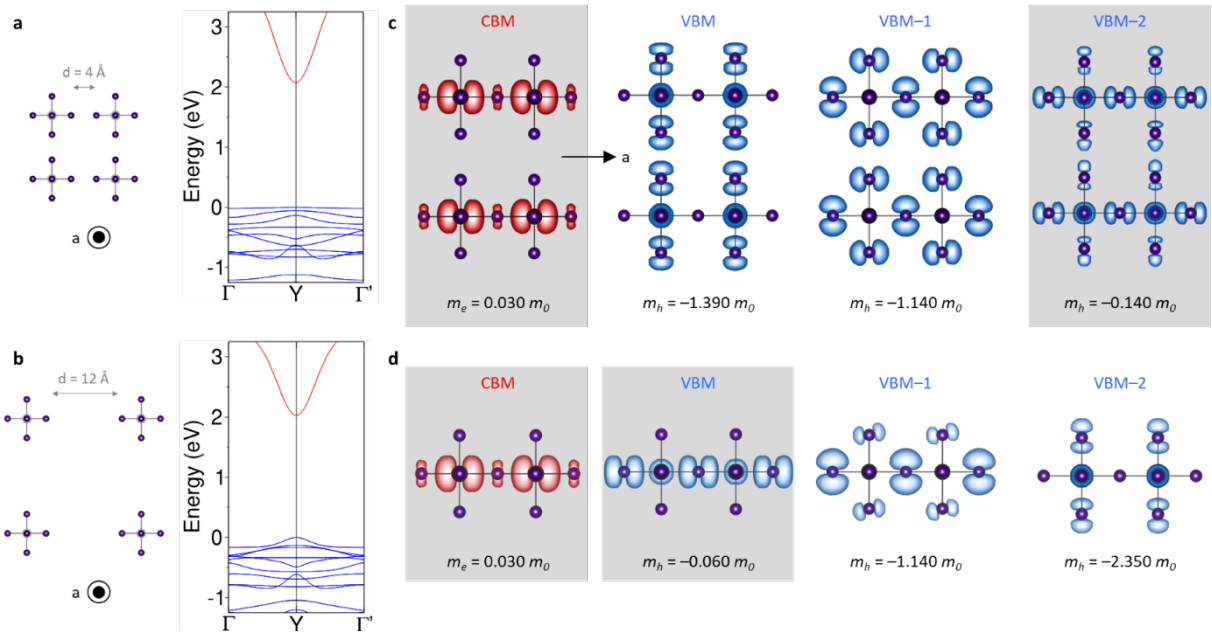

Figure S11. Electronic properties of trans-connected PbI_5 model structures. (a) Band structure of the model PbI_5-chains with short 4 Å inter-chain distance computed using the revPBE functional and a background charge to mimic the effect of organic cations. The origin of the energy scale is taken at the top of the valence band. (b) Same with the model PbI_5-chains with increased (12 Å) inter-chain distance. (c) Wavefunctions modulus taken at the conduction band maximum (red), valence band maximum (blue) and next lower lying valence bands (blue) computed for the 4 Å model. The corresponding electron and hole effective masses are given below. (d) Same for the 12 Å model. Considering the large distance between chains, only a single chain is depicted. The gray areas mark states with low effective masses. In both configurations, CBMs consist in overlapping Pb($6p_x$) orbitals leading to highly dispersive bands and small electron effective masses. In the short inter-chain distance model, the VBM consists in inter-chain couplings between dangling iodides and a large hole effective mass along the chain. In the long-distance model, this valence state is lowered in energy and the VBM is formed by intra-chain couplings. By contrast with the Bi-chain, the efficient coupling between I($5p_x$) and Pb($6s$) orbitals leading to low hole effective masses becomes the top valence band. As a consequence, the hole transporting properties of the isolated *trans*-connected PbI_5 chains are considerably improved.

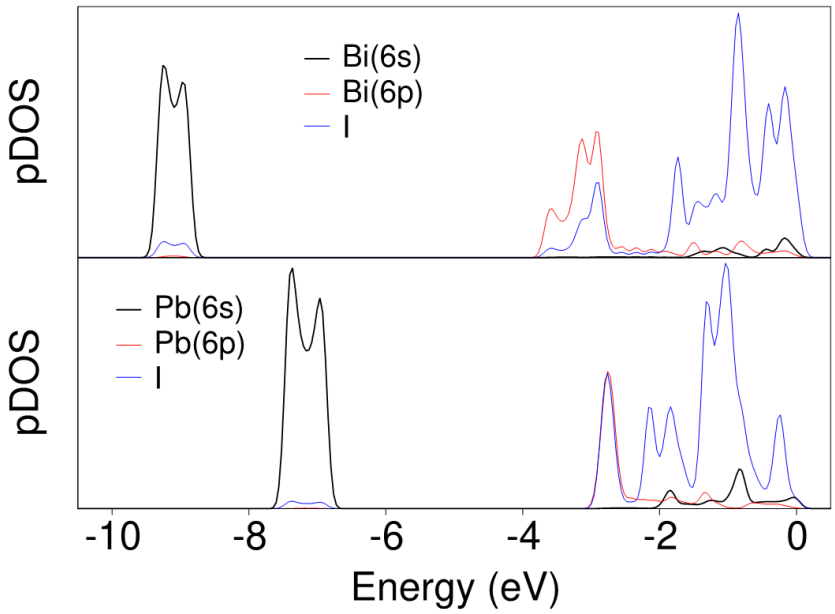

Figure S12. Projected density of states (pDOS) of *trans*-connected MI_5 model structures (M=Bi, Pb). BiI_5 (top) and PbI_5 (bottom) isolated wires computed using the revPBE functional and a background charge to keep charge neutrality, i.e. mimic the presence of organic cations. The origin of the energy scale is taken at the top of the valence band. Bi(*6s*) and Pb(*6s*) contributions have been multiplied by 2 to improve readability. The reduced Pb(*6s*)-Pb(*6p*) splitting with respect to the Bi(*6s*)-Bi(*6p*) one, increase the energy of the anti-bonding coupling between *6s* metal orbitals and $6p_x$ bridging iodine orbitals leading to the highly efficient hole transporting state that then becomes the VBM in the case of PbI_5 chain.

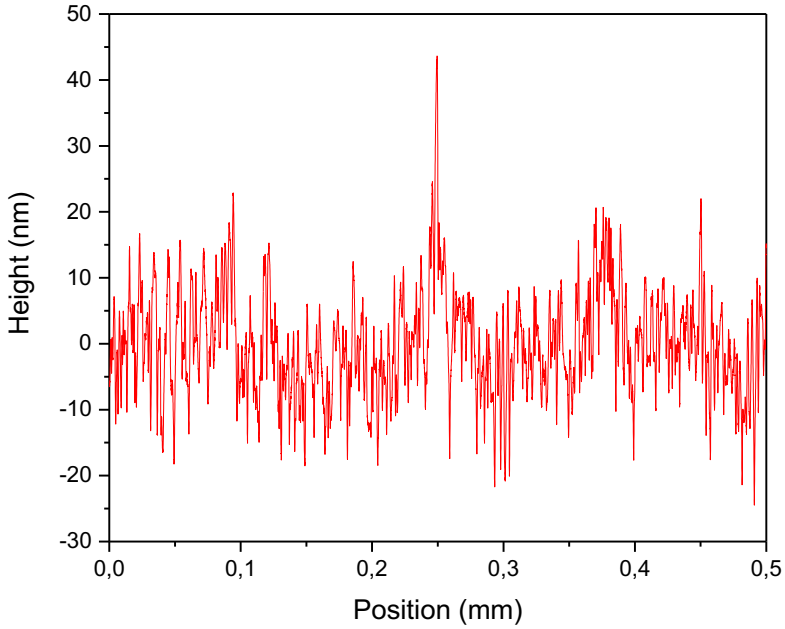

Figure S13. Profilometry measurement of a thin film of (AmV)BiI_5.